Supporting Information

Direct Aminolysis of Methyl Esters With Ammonia in Continuous Flow Through Bayesian Optimization

*Bavo Vandekerckhove,[a] Stefan Desimpel,[a] Bart Ruttens,[b] Massimo Bocus,[c] Wim Temmerman,[c] Bert Metten,[b] Veronique Van Speybroeck,[c] Thomas S.A. Heugebaert,[a] Christian V. Stevens[a]**

[a] SynBioC Research Group, Department of Green Chemistry and Technology, Faculty of Bioscience Engineering, Ghent University, Coupure Links 653, B-9000 Ghent, Belgium

[b] Ajinomoto Bio-Pharma Services, Cooppallaan 91, 9230 Wetteren, Belgium

[c] Center for Molecular Modeling, Tech Lane Ghent Science Park, Campus Ardoyen, Ghent University, Technologiepark 46, 9052 Zwijnaarde, Belgium

*Chris.Stevens@UGent.be

General information

All reagents (methyl picolinate, ammonia solution etc.) were purchased from TCI Europe or BLDpharm and used as such. NMR spectra were measured with a Bruker Avance Nanobay III NMR spectrometer. The components were dissolved in deuterated DMSO-d_6 or D_2O and tetramethylsilane (TMS) as an internal standard. Microwave reactions were performed in a CEM FocusedTM Microwave Synthesis sistem, Model Discover, with adaptable power from 0-300 W, monitored with the Synergy-software V. 1.32 (maximum temperature = 250 °C, macimum pressure = 21 bar). For the measurement of the water content, The C10S Karl-Fisher Coulometer from Mettler Toledo was used.

Aminolysis in batch

In a flame dried microwave vial (10 mL) equipped with a magnetic stirrer, 150 mg of methyl picolinate is combined with 12 equivalents of ammonia in MeOH (7 N) (1.9 mL). The vial is tightly sealed (PTFE septum) and placed in the microwave reactor at 130 °C for 10 minutes while stirring. Subsequently, the solvent is evaporated and ^{1}H-NMR analysis is conducted using dimethyl sulfone as the internal standard, and both the conversion and NMR yield are determined. Experiments with different time/temperature conditions were conducted in a similar manner.

Computational analysis

To elucidate the factors that might influence the observed experimental yields, we performed an additional theoretical investigation and explore the energetics of the reaction. We started by localizing the most stable conformer of each molecule (17 methyl esters, **1a**–**1q** and the corresponding amides **2a**–**2q**), as most of them are expected to be relatively flexible. To this end, we used the iMTD-GC workflow implemented in the CREST 3.0.2 software at a GFN2-xTB level of theory [1-3]. We performed both a conformational search in gas-phase and one in methanol with an implicit solvation model, using a generalized Born model with surface area contributions method implemented in CREST.

After obtaining a conformer list for each of the molecules, we moved to a more accurate description of the potential energy surface (PES). For each molecule, we selected all conformers that, according to GFN2-xTB, were within 2 kcal·mol^{-1} from the most stable one, with a maximum of 10 conformers per molecule. These were fully reoptimized at a B3LYP-D3(BJ)/def2-TZVP level of theory within the Gaussian16 (revision C.02) software [4-8]. Each molecule was characterized by a normal mode analysis to ensure that a minimum on the PES

was effectively reached. If any structure presented a significant imaginary frequency, the atoms were displaced along the imaginary normal mode and then fully reoptimized, until a minimum was reached. The procedure was, as for the conformer search, performed both in gas-phase and in implicit methanol using the default SCRF method implemented in Gaussian [9]. Methanol and ammonia were also optimized and the reaction energy for each identified stable conformer was calculated as:

$$\Delta E = E(RNH_2) + E(MeOH) - (E(ROMe) + E(NH_3))$$

Equation S1. Calculation of the energy difference between products and reagents.

Continuous flow setup

Figure S1 illustrates a schematic overview of the continuous flow setup, denoted as the CØPE reactor. One Teledyne ISCO HLf 500d was used as pressure resistant pump to precisely dose the flow into the reactor. The system pressure is indicated by this pump on the display interface. Adjustments of the pulsator amplitude can be made using the rotary knob, ranging from 0.0 to 0.95 in increments of 0.05. These values correspond to a percentage of the maximum stroke volume, which is 0.76 mL/stroke (or a maximum stroke amplitude of 0.38 mL/stroke). The frequency of the strokes is controlled using the Danfoss VLT® Midi Drive FC 280 frequency controller. N_2 gas from an external gas tank pressurizes the cylindrical BPR to achieve the desired system pressure.

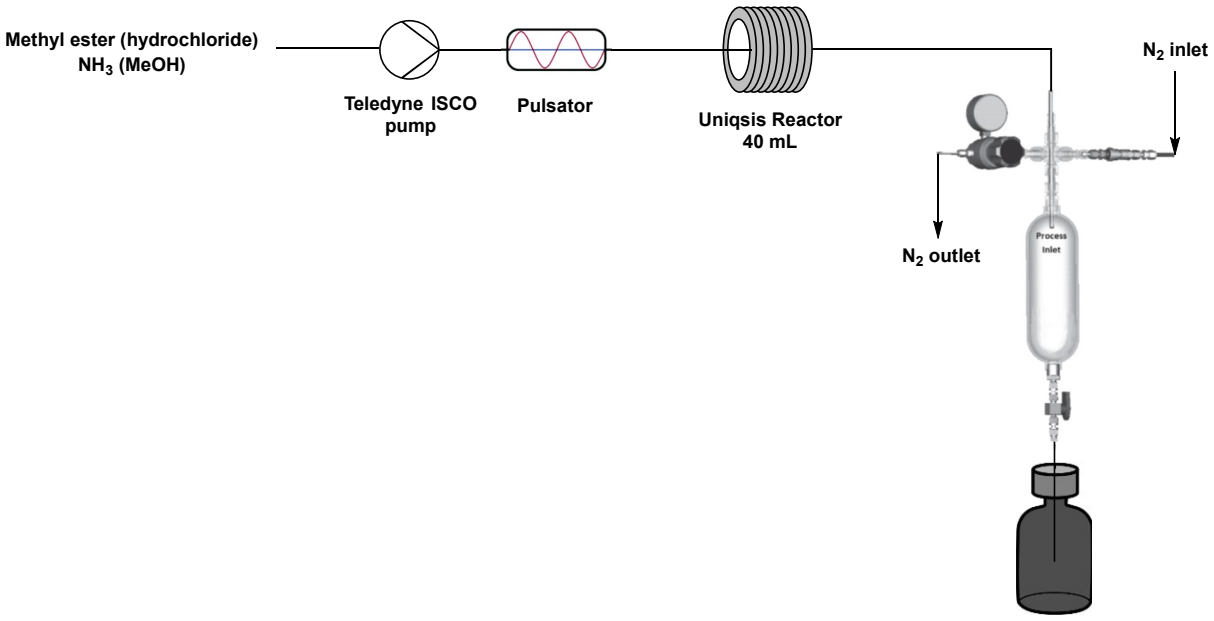

Figure S1. Schematic overview of the continuous flow setup (CØPE reactor).

Figure S2. Photograph of the continuous flow setup (CØPE Reactor; A: pump (Teledyne Isco Hlf 500d); B: pulsator; C: reactor (Uniqsis); D: BPR; E: collection vessel).

Aminolysis in continuous flow

Initially, a feed vessel is prepared by mixing 6.72 grams of methyl picolinate with 140 mL methanolic ammonia (7 N solution, 20 eq.). The mixture is stirred and the Teledyne ISCO syringe pump is filled with the solution. Before the reaction is started, the system undergoes methanol flushing and pressurization to 15 bar. A flow rate of 1.333 mL/min is programmed, translating to a residence time of 30 minutes. Upon reaching steady state after three times the

residence time, the cylindrical collection vessel is emptied to prevent contamination of the samples. Subsequently, two samples are collected and analyzed using the same analytical procedure as in the batch process. The reported conversion and NMR yield represent the average of both samples.

Bayesian Optimization

For a detailed explanation of the MVMOO algorithm, we refer readers to its original publication [10] and a previous application in chemical reaction optimization [11]. In summary, the algorithm employs a Gaussian process (GP) as a surrogate model for each objective. A GP is a non-parametric regression model that can be viewed as an infinite-dimensional generalization of a multivariate Gaussian distribution. A key feature of the MVMOO algorithm is its use of GPs with an internal distance metric based on Gower similarity, allowing it to handle mixed-variable optimization. The algorithm can be initialized with any small dataset, though a common choice is a small Latin Hypercube Sampling (LHS) to ensure a space-filling design. The hyperparameters of each GP are optimized to achieve the best fit to the data. Next, the Expected Improvement Matrix (EIM) acquisition function is constructed from the GPs and optimized to determine the next set of reaction conditions. After conducting the experiment, the results are incorporated into the dataset, the GPs are updated, and the process is repeated iteratively until termination criteria are met. In Bayesian optimization, termination typically occurs after a fixed number of iterations or when the user is satisfied with the results.

Some modifications were made to the algorithm to enable its use in systems with only continuous variables, as previously reported by our group [12]. The GitHub version available as of July 2024 contained a minor bug that caused an error in such cases. The specific changes made to address this issue are summarized in Table S1.

Line	**Original**	**Change**
multi_mixed_optimiser.py – line 351	results.append(stats.optimize.minimize(self.EIMoptimiserWrapper, xmax[i,:-self.num_qual].reshape(-1), args=(qual[i],constraints,modes[i]), bounds=bndlist,method='SLSQP'))	Replaced *:-self.num_qual* by *:self.-num_quant*, otherwise the slicing when num_qual = 0 is incorrect.
multi-mixed_optimiser.py – line 363	qual = xmax[-self.num_qual:]	*if self.num_qual == 0:* *qual = np.array([])* *else:* *qual = xmax[-self.num_qual:]* Slicing issue when num_qual = 0,

		because then qual would be xmax, even though there are no qualitative variables.
multi-mixed_optimiser.py – line 371	result = stats.optimize.minimize(self.EIMoptimiserWrapper, xmax[:-self.num_qual].reshape(-1), args=(qual,constraints,mode), bounds=bndlist,method='SLSQP')	Replaced *:-self.num_qual* by *:self.-num_quant*, otherwise the slicing when num_qual = 0 is incorrect.

Table S1. Changes made to the MVMOO algorithm, according to Desimpel et al [12].

Substrate analysis

Prolinamide hydrochloride **2a**

Purification: after evaporation of the solvent, the residue was recrystallized in isopropanol. The obtained solids were filtered off and dried. During screening, NMRs were taken in D_2O, the final product was analyzed with DMSO-d_6.

^{1}H-NMR (400MHz, DMSO-d_6): δ 9.23 (2H, s, -NH-HCl), 8.09 (1H, s, -NH_2), 7.62 (1H, s, -NH_2), 4.11 (1H, m, C_{quat}-CH), 3.18 (2H, m, NH-CH_2), 2.29 (1H, m, C_{quat}-CH-CH_2), 1.85 (3H, m, C_{quat}-CH-CH_2, CH_2-CH_2-CH_2) ppm (isolated)

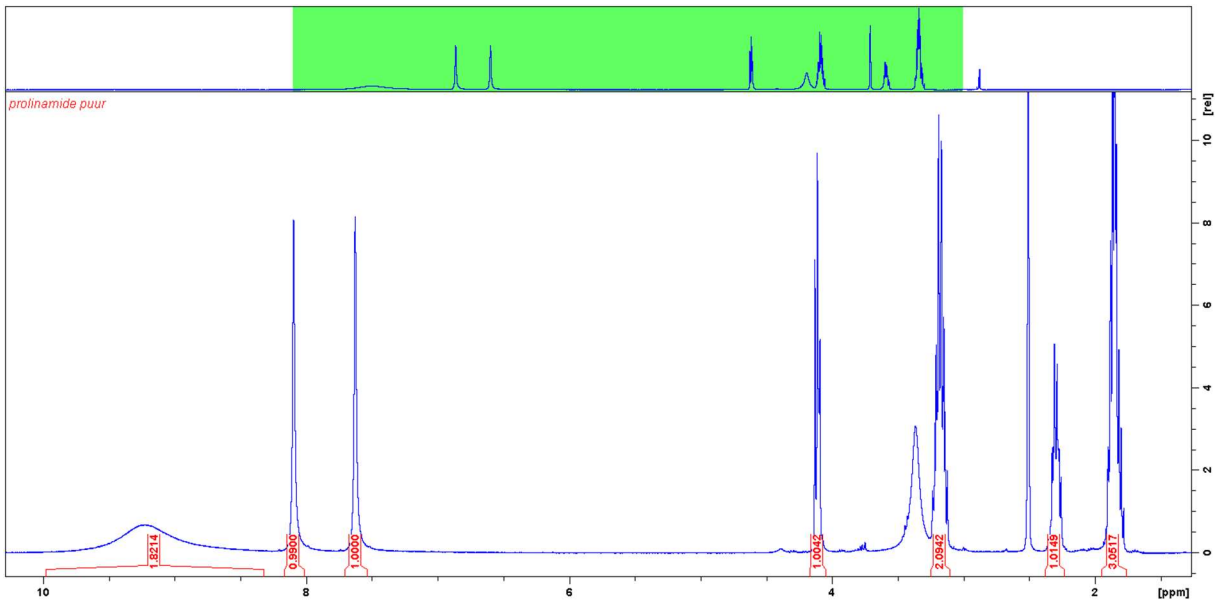

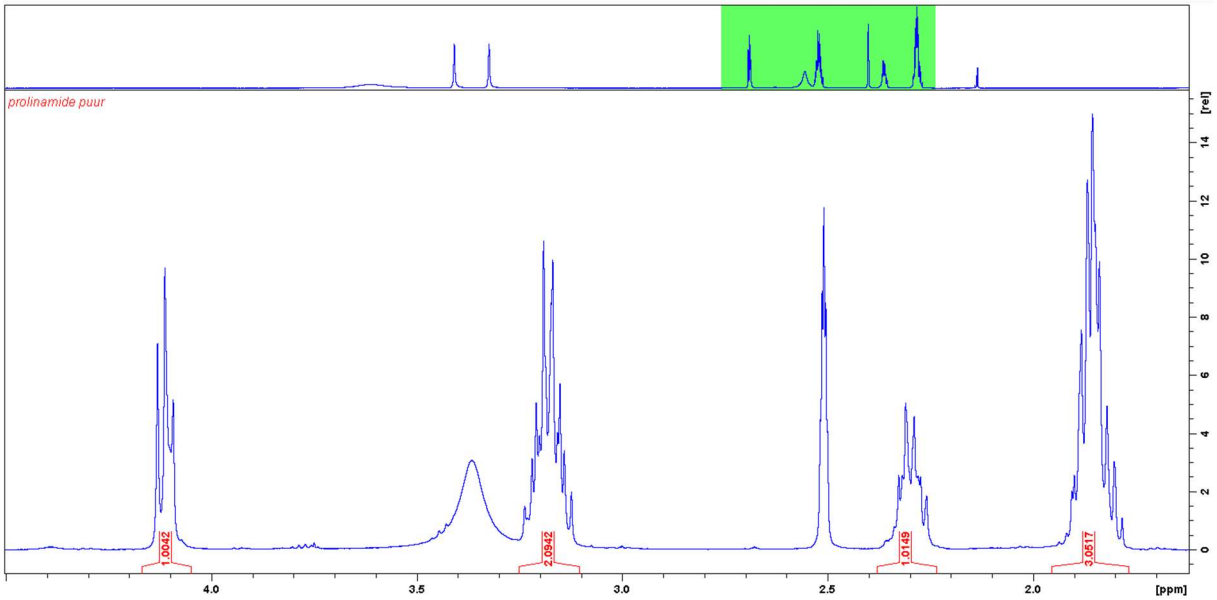

Figure S3. ^{1}H-NMR of prolinamide hydrochloride in DMSO-d_6.

Picolinamide **2b**

Purification: after evaporation of the solvent, the residue was recrystallized in EtOH. The obtained solids were filtered off and dried.

^{1}H-NMR (400MHz, DMSO-d_6): δ 8.64 (1H, s, N=C<u>H</u>), 8.12 (1H, s, -N<u>H</u>$_2$), 8.05 (1H, d, C_{quat}-C<u>H</u>), 7.98 (1H, t, =C<u>H</u>), 7.65 (1H, s, -N<u>H</u>$_2$), 7.59 (1H, t, =C<u>H</u>) ppm (isolated)

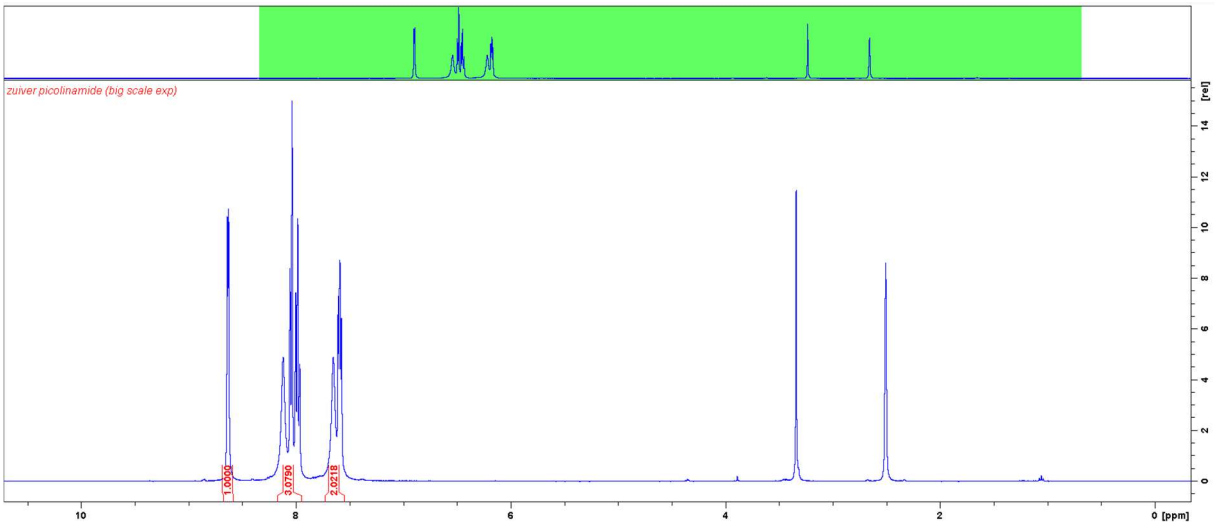

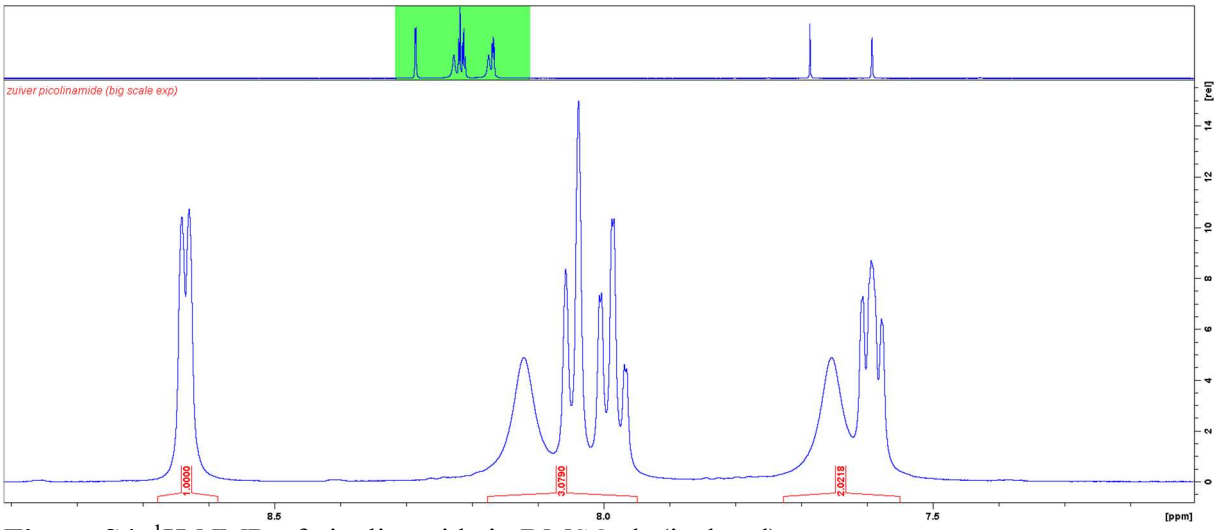

Figure S4. ^{1}H-NMR of picolinamide in DMSO-d_6 (isolated).

Piperidine-2-carboxamide hydrochloride **2i**

Purification: after evaporation of the solvent, the residue was recrystallized in EtOH. The obtained solids were filtered off and dried.

^{1}H-NMR (400MHz, DMSO-d_6): δ 8.95 (2H, s, -N<u>H</u>-<u>H</u>Cl), 7.96 (1H, s, -N<u>H</u>$_2$), 7.55 (1H, s, -N<u>H</u>$_2$), 3.68 (1H, m, -C<u>H</u>-C$_{quat}$), 3.18 (1H, m, C$_{quat}$-CH-C<u>H</u>$_2$), 2.87 (1H, m, C$_{quat}$-CH-C<u>H</u>$_2$), 2.13 (1H, m, C$_{quat}$-NH-C<u>H</u>$_2$), 1.61 (5H, m, C$_{quat}$-NH-C<u>H</u>$_2$, -C<u>H</u>$_2$-C<u>H</u>$_2$-) ppm (isolated)

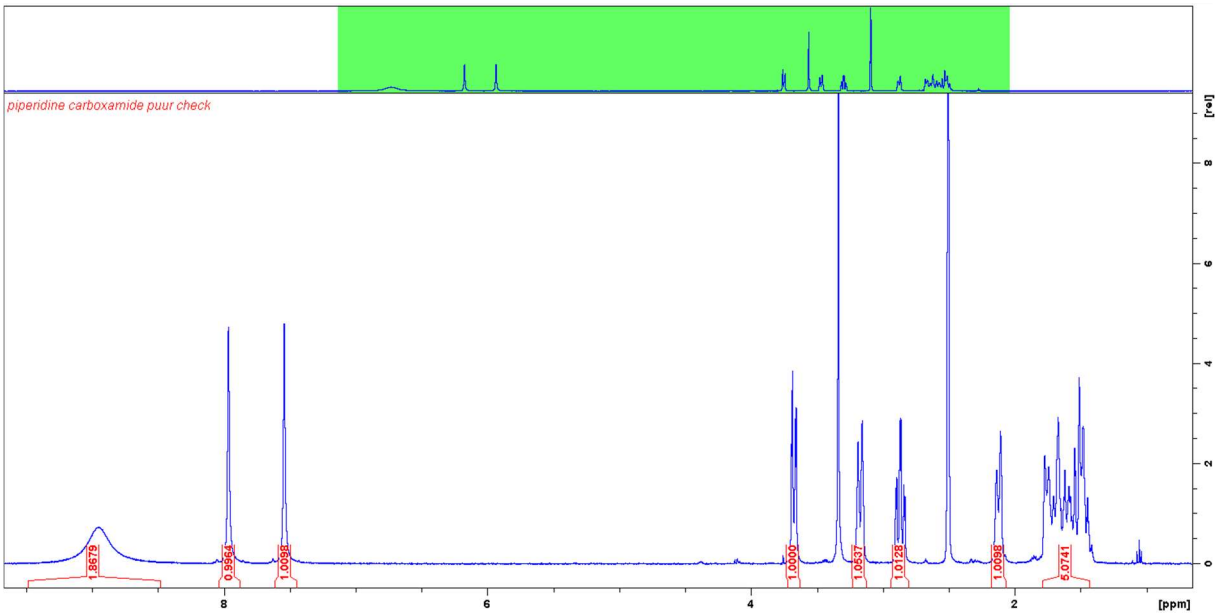

Figure S5. ^{1}H-NMR of piperidine-2-carboxamide hydrochloride in DMSO-d_6 (isolated).

Tetrahydrofuran-2-carboxamide **2k**

Purification: after evaporation of the solvent, the residue was recrystallized in isopropanol. The obtained solids were filtered off and dried.

^{1}H-NMR (400MHz, DMSO-d_6): δ 7.15 (2H, d, -N<u>H</u>$_2$), 4.13 (1H, m, C_{quat}-C<u>H</u>), 3.88 (1H, m, C<u>H</u>$_2$-O), 3.74 (1H, m, C<u>H</u>$_2$-O), 2.09 (1H, m, C_{quat}-CH-C<u>H</u>$_2$), 1.81 (3H, m, C_{quat}-CH-C<u>H</u>$_2$, CH$_2$-C<u>H</u>$_2$-CH$_2$) ppm (isolated)

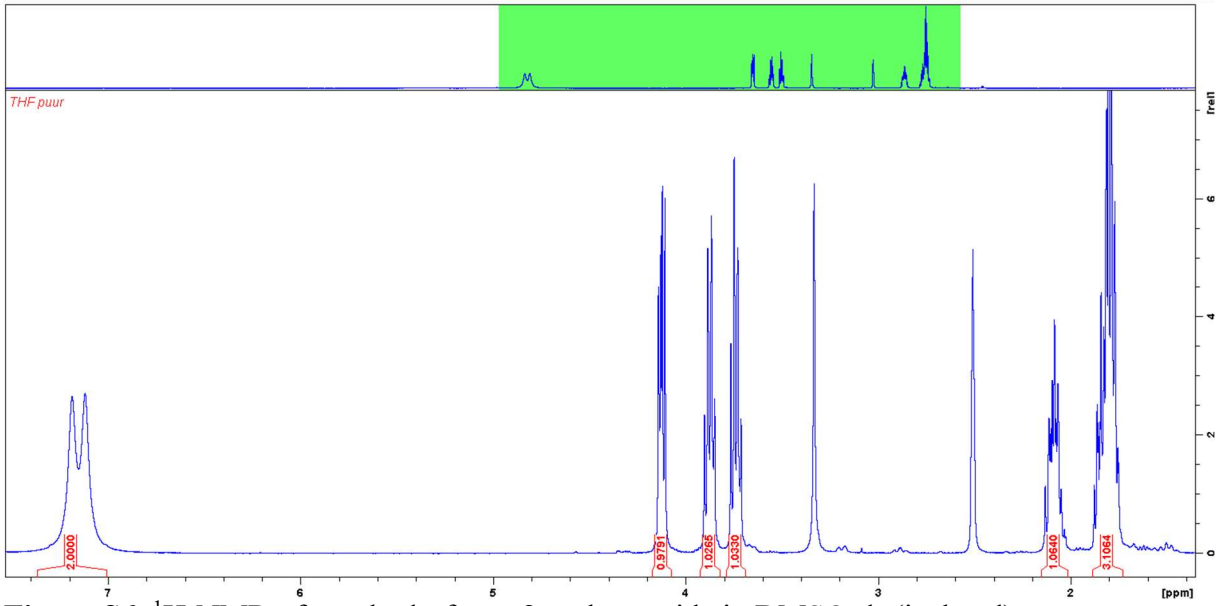

Figure S6. ^{1}H-NMR of tetrahydrofuran-2-carboxamide in DMSO-d_6 (isolated).

4-methoxypicolinamide **2q**

Purification: after evaporation of the solvent, the residue was recrystallized in EtOH. The obtained solids were filtered off and dried.

^{1}H-NMR (400MHz, DMSO-d_6): δ 8.44 (1H, d, N=C<u>H</u>), 8.09 (1H, s, -N<u>H</u>$_2$), 7.66 (1H, s, -N<u>H</u>$_2$), 7.56 (1H, d, C_{quat}=C<u>H</u>-C_{quat}), 7.14 (1H, dxd, OMe-C_{quat}=C<u>H</u>) ppm (isolated)

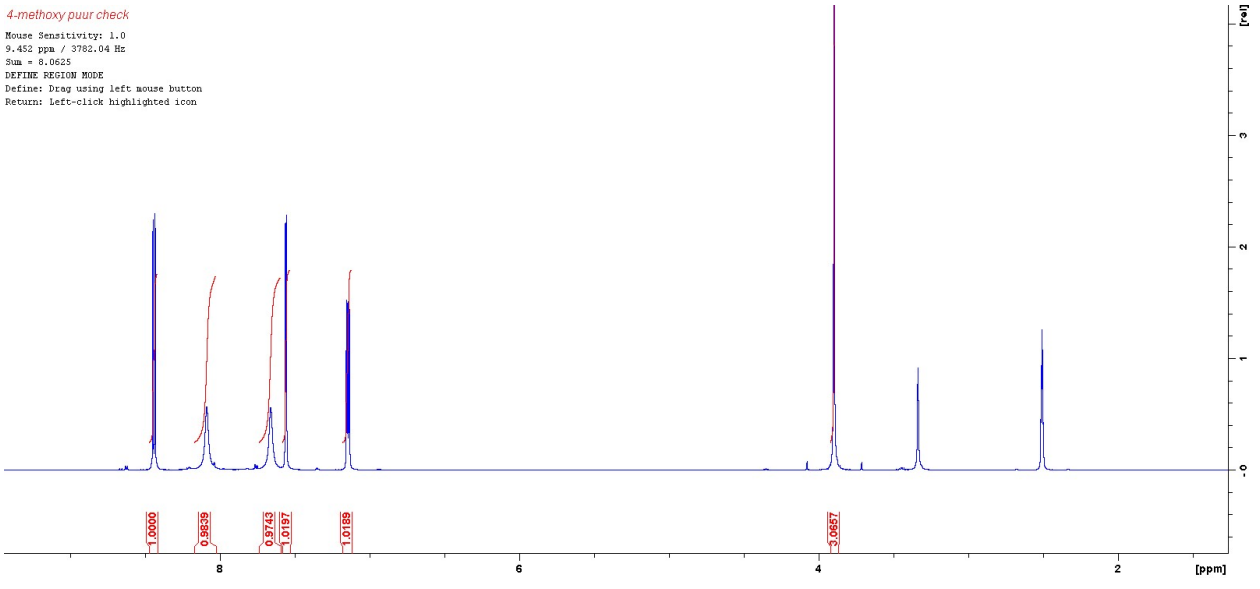

Figure S7. ^{1}H-NMR of 4-methoxypicolinamide in DMSO-d_6 (isolated).

Sources

[1] Pracht, P., Bohle, F., Grimme, S., Automated exploration of the low-energy chemical space with fast quantum chemical methods, journal of physical chemistry chemical physics, 2020, 22, 7169-7192, https://doi.org/10.1039/C9CP06869D

[2] Pracht, P., Grimme, S., Bannwarth, C., Bohle, F., Ehlert, S., Feldmann, G., Gorges, J., Müller, M., Neudecker, T., Plett, C., Spicher, S., Steinbach, P., Wesołowski, P.A., Zeller, F., CREST—A program for the exploration of low-energy molecular chemical space, J. Chem. Phys., 2024; 160 (11): 114110. https://doi.org/10.1063/5.0197592

[3] Bannwarth, C., Ehlert, S., Grimme, S., GFN2-xTB—An Accurate and Broadly Parametrized Self-Consistent Tight-Binding Quantum Chemical Method with Multipole Electrostatics and Density-Dependent Dispersion Contributions, J. Chem. Theory Comput., 2019, 15, 3, 1652–1671, https://doi.org/10.1021/acs.jctc.8b01176

[4] Weigend, F., Accurate Coulomb-fitting basis sets for H to Rn, Journal of Physical Chemistry Chemical Physics, 2006, 8, 1057-105, https://doi.org/10.1039/B515623H

[5] Weigend, F., Ahlrichs, R., Balanced basis sets of split valence, triple zeta valence and quadruple zeta valence quality for H to Rn: Design and assessment of accuracy, Journal of Physical Chemistry Chemical Physics, 2005, 7, 3297-3305, https://doi.org/10.1039/B508541A

[6] Grimme, S., Ehrlich, S., Goerigk, L., Effect of the damping function in disperion corrected density functional theory, Journal of computational chemistry, 2011, 32, 1456-1465, https://doi.org/10.1002/jcc.21759

[7] Grimme, S., Antony, J., Ehrlich, S., Krieg, H., A consistent and accurate ab initio parametrization of density functional dispersion correction (DFT-D) for the 94 elements H-P, J. Chem. Phys., 2010, 132 (15), 154104, https://doi.org/10.1063/1.3382344

[8] Gaussian 16, Revision C.02, M. J. Frisch, G. W. Trucks, H. B. Schlegel, G. E. Scuseria, M. A. Robb, J. R. Cheeseman, G. Scalmani, V. Barone, G. A. Petersson, H. Nakatsuji, X. Li, M. Caricato, A. V. Marenich, J. Bloino, B. G. Janesko, R. Gomperts, B. Mennucci, H. P. Hratchian, J. V. Ortiz, A. F. Izmaylov, J. L. Sonnenberg, D. Williams-Young, F. Ding, F. Lipparini, F. Egidi, J. Goings, B. Peng, A. Petrone, T. Henderson, D. Ranasinghe, V. G. Zakrzewski, J. Gao, N. Rega, G. Zheng, W. Liang, M. Hada, M. Ehara, K. Toyota, R. Fukuda, J. Hasegawa, M. Ishida, T. Nakajima, Y. Honda, O. Kitao, H. Nakai, T. Vreven, K. Throssell, J. A. Montgomery, Jr., J. E. Peralta, F. Ogliaro, M. J. Bearpark, J. J. Heyd, E. N. Brothers, K. N. Kudin, V. N. Staroverov, T. A. Keith, R. Kobayashi, J. Normand, K. Raghavachari, A. P. Rendell, J. C. Burant, S. S. Iyengar, J. Tomasi, M. Cossi, J. M. Millam, M. Klene,

C. Adamo, R. Cammi, J. W. Ochterski, R. L. Martin, K. Morokuma, O. Farkas, J. B. Foresman, and D. J. Fox, Gaussian, Inc., Wallingford CT, 2016

[9] Tomasi, J., Mennucci, B., Cammi, R., Quantum Mechanical Continuum Sovation Models, Chemical Reviews, 2005, 105, 8, 2999-3094, https://doi.org/10.1021/cr9904009

[10] Manson, J.A., Chamberlain, T.W., Bourne, R.A., MVMOO: Mixed variable multi-objective optimisation, Journal of Global Optimization, 2021, 80, 865–886, https://doi.org/10.1007/S10898-021-01052-9/FIGURES/10.

[11] Kershaw, O.J., Clayton, A.D., Manson, J.A., Barthelme, A., Pavey, J., Peach, P., Mustakis, J., Howard, R.W., Chamberlain, T.W., Warren, N.J., Bourne, R.A., Machine learning directed multi-objective optimization of mixed variable chemical systems, Chemical Engineering Journal, 2023, 451, 138443, https://doi.org/10.1016/j.cej.2022.138443.

[12] Desimpel, S., Dijkmans, J., Kuijpers, K.P.L., Dorbec, M., Van Geem, K.M., Stevens, C.V., Efficient multi-objective Bayesian optimization of gas-liquid photochemical reactions using an automated flow platform, Chemical Engineering Journal, 2024, 501, https://doi.org/10.1016/j.cej.2024.157685